Materials Science and Engineering A 528 (2011) 7488–7493

Contents lists available at ScienceDirect

Materials Science and Engineering A

journal homepage: www.elsevier.com/locate/msea

Dynamic recrystallization behavior of a superaustenitic stainless steel containing 16%Cr and 25%Ni

G.R. Ebrahimi [a,*], H. Keshmiri [a], A. Momeni [b], M. Mazinani [c]

[a] Department of Materials Engineering, Sabzevar Tarbiat Moallem University, Sabzevar, Iran
[b] Department of Mining and Metallurgy, Amir Kabir University of Technology, Tehran, Iran
[c] Department of Materials Engineering, Faculty of Engineering, Ferdowsi University of Mashhad, Mashhad, Iran

ARTICLE INFO

Article history:
Received 18 November 2010
Received in revised form 18 April 2011
Accepted 31 May 2011
Available online 12 June 2011

Keywords:
Hot deformation
Dynamic recrystallization
Solute drag
Critical strain

ABSTRACT

Dynamic recrystallization behavior of austenite in a superaustenitic stainless steel containing 16%Cr and 25%Ni was studied using hot compression tests in a temperature range of 900 °C–1200 °C and at strain rate of 0.001 s^{-1}– 1s^{-1}. The initiation and evolution of dynamic recrystallization were investigated by microstructural analysis. The effect of deformation temperature and strain rate on the flow stress during dynamic recrystallization was studied using the hyperbolic sine equation. The apparent activation energy for the hot deformation was calculated to be about 484 kJ/mol. Dynamic recrystallization was delayed when the logarithm of the Zener–Hollomon parameter fell within 13–15 s^{-1}. This retardation was attributed to the segregation of substitutional impurity elements, mainly phosphorus, to grain boundaries where recrystallization is originally initiated.

1. Introduction

Hot deformation is employed to optimize the microstructure and mechanical properties of different steel grades. Being very important from the industrial point of view, stainless steels have drawn great attention concerning their hot deformation behavior. Among the vast family of stainless steels the hot deformation behavior of superaustenitic grades has been less investigated; even though they provide very important industrial applications [1].

It has been understood that dynamic recrystallization (DRX) is the dominant restoration mechanism for stainless steels which are hot deformed in the stability region of austenite [2–8]. DRX often occurs during the hot working of metals and alloys with low or medium stacking fault energy (SFE). When SFE is low, e.g. in case of austenite, the cross-slip of dislocations does not occur easily. This gives rise to a slow dynamic recovery during deformation [9] and therefore accumulative increase in the dislocation density until starting DRX [10].

DRX often originates from high angle boundaries (HABs) by the nucleation and growth of new strain-free grains [11,12]. HABs may be the original grain boundaries, the boundaries of dynamically recrystallized grains or the boundaries created during straining such as deformation bands or shear bands. The local bulging of grain boundaries is frequently observed as a prelude to dynamic recrystallization [10].

Inasmuch as DRX leads to the formation of new grains, it is often treated as a potential way to the microstructural control aimed at the controlled thermomechanical processes such as controlled rolling or forging [2]. Undoubtedly, the kinetics and extent of DRX process strongly depend on two variables, materials characteristics and processing parameters. These may control the mobility of HABs and therefore the easiness of the initiation of DRX. In this regard, the dragging effect of segregating solute atoms and the pinning influence of strain induced second phase particles to the HABs are known to effectively postpone or even inhibit DRX [1,13]. Some previous investigations have reported the interaction of DRX with segregating solute atoms to HABs in low carbon and microalloyed steels [13–15]. It is often observed that the affinity between HABs and segregated solute atoms decreases the boundary mobility and contributes therefore in the retardation of DRX. Given profound investigations regarding the solute drag effect but it has been less noted in the hot deformation of stainless steels. The present research is therefore devoted to investigate the hot deformation behavior of a 16%Cr–25%Ni superaustenitic stainless steel with special attention to the interaction of DRX with solute dragging effect.

2. Experimental procedure

The material used in this investigation was Cr16Ni25Mo6 superaustenitic stainless steel with the chemical composition given in

* Corresponding author. Tel.: +98 571 4003520; fax: +98 571 4003527.
E-mail addresses: ebrahimi@sttu.ac.ir, r_ebrahimi2000@yahoo.com (G.R. Ebrahimi).

0921-5093/$ – see front matter © 2011 Elsevier B.V. All rights reserved.
doi:10.1016/j.msea.2011.05.081

Table 1
Chemical composition of the stainless steel used in this research.

component	C	*Cr*	Ni	Mo	P	S	Si
wt%	0.04	16.10	25.50	5.80	0.03	0.015	0.72

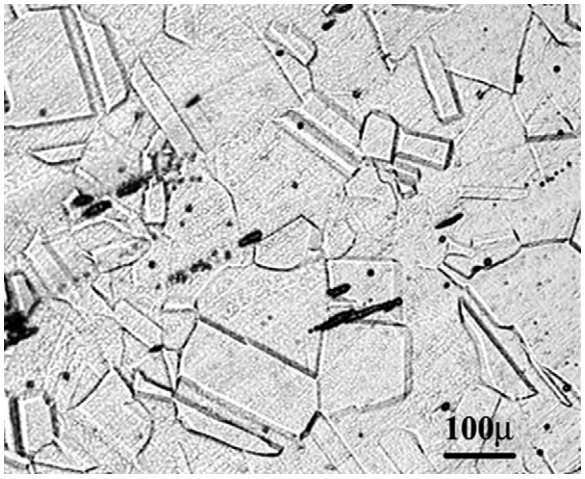

Fig. 1. Starting microstructure of the austenitic stainless steel used in this investigation.

Table 1. According to the as-received microstructure shown in Fig. 1 the initial grain size was determined to be about 160 μm. Cylindrical compression samples of 12 mm height and 8 mm diameter were prepared from the as-received hot forged bar according to the ASTM E209 standard. In order to minimize the effect of friction and to keep the boron nitride as the lubricant material between the contacting surfaces of samples and anvils some concentric grooves of 0.5 mm depth were machined on the both surfaces of each sample. A Zwick Roell 250 hot deformation machine was used to perform hot compression tests at constant strain rates. Before testing, all the specimens were reheated to 1200 °C, held for 5 min and cooled down to testing temperature. This procedure was performed to simulate the industrial hot working processes such as hot forging. After soaking for 3 min at testing temperature, continuous hot compression tests were carried out in a temperature range of 900 °C–1200 °C and at strain rates ranging from 0.001 s^{-1} to 1 s^{-1} at an interval of an order of magnitude. The samples immediately quenched after hot compression to preserve the microstructure for the investigation of DRX. The water quenched specimens were sectioned longitudinally and polished with 1 μm diamond paste and then electrolytically etched in a solution of 10% hydrochloric acid in pure water to reveal their microstructure.

3. Results and discussion

Single-hit hot compression tests were conducted at various strain rates and four different temperatures. Fig. 2(a) shows typical true stress–strain curves indicating the effect of temperature on flow stress at a given strain rate of 0.01 s^{-1}. As expected, the flow stress value clearly declines with temperature. The influence of strain rate at temperature of 1050 °C, is shown in Fig. 2(b) manifesting the fact that flow stress level increases as strain rate rises. Flow curves of Fig. 2(a) and (b) are obviously typical of DRX. They are characterized by work hardening up to a peak following which flow stress decreases until reaching the plateau of steady state region.

In order to characterize a typical flow curve of DRX the critical and peak strains are commonly determined from the stress–strain data [16–18]. The critical strain required for the initiation of DRX can be identified as the inflection point of the θ–σ curve (where

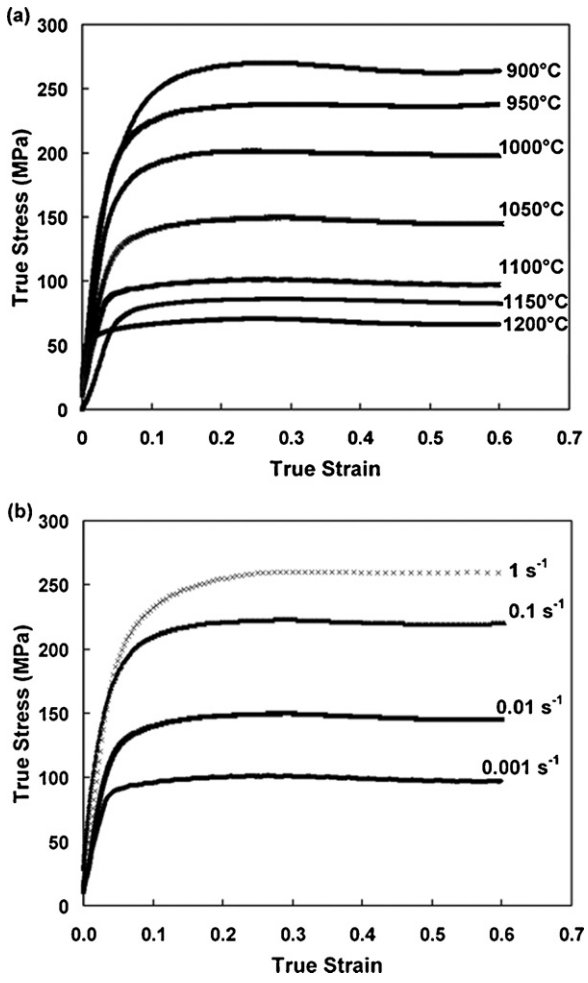

Fig. 2. Representative stress–strain curves of the studied material (a) strain rate of 0.01 s^{-1} and (b) temperature of 1050 °C.

$\theta = d\sigma/d\varepsilon$) [19–22]. One way to follow the microstructural events during hot deformation is monitoring the changes in the value of θ with respect to strain or stress. As seen in Fig. 3, when θ is depicted vs. true stress, three regions are discernible. In the first region, the work hardening rate linearly decreases with stress to σ_{sub} which is known as the required stress for the formation of sub-structure. In the second region, the slope decreases until reaching a point at

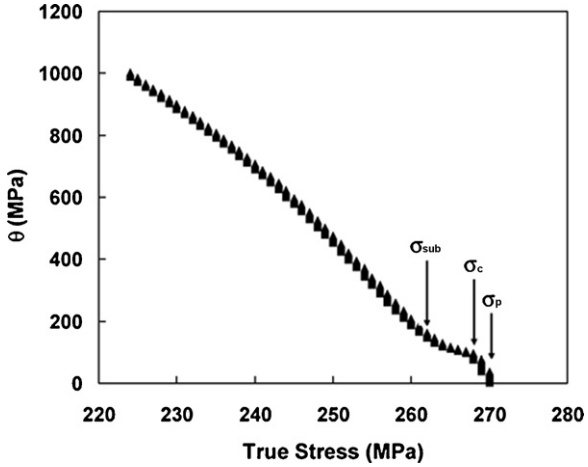

Fig. 3. Variation of work hardening rate vs. true stress at 900 °C and 0.01 s^{-1}.

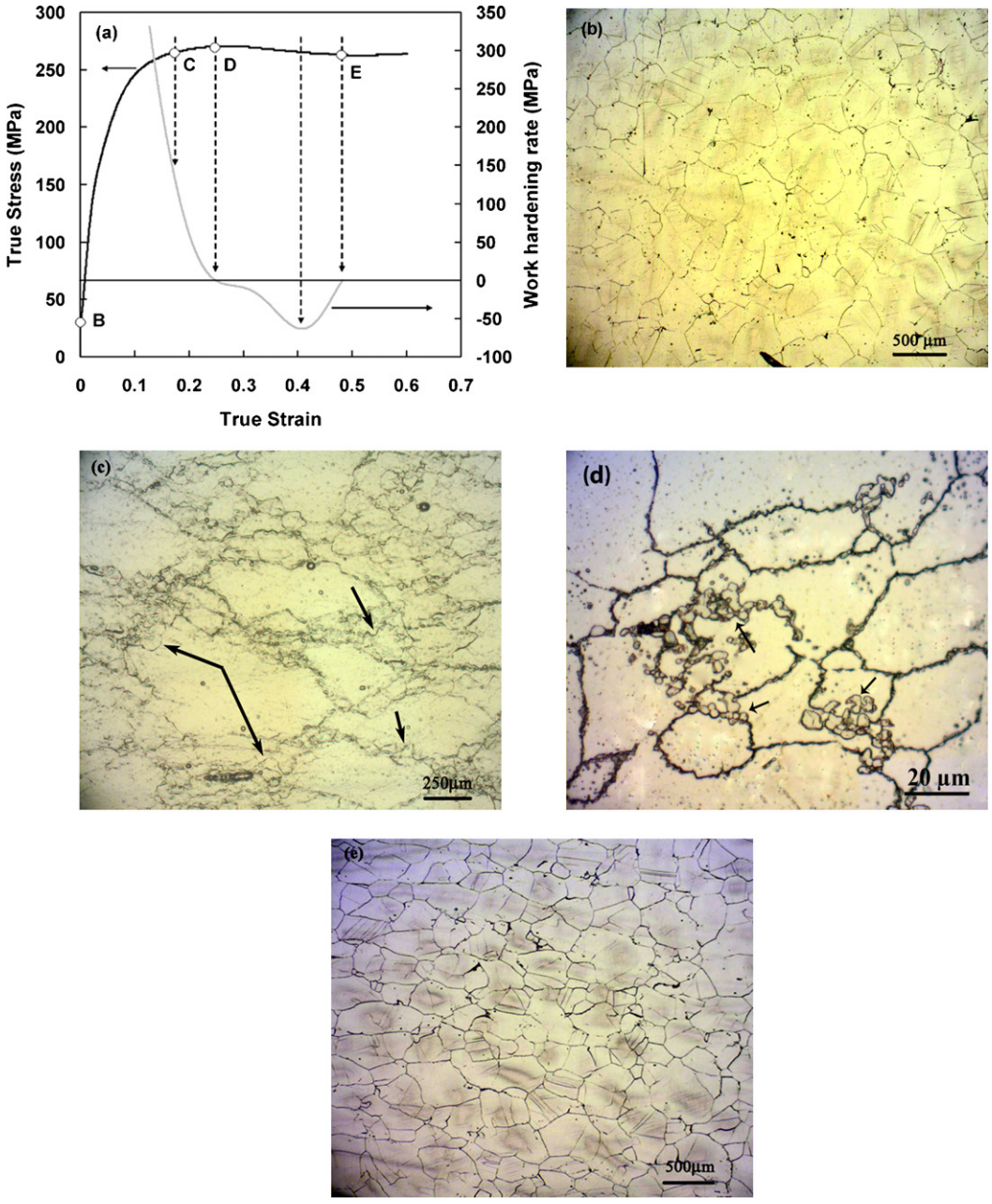

Fig. 4. (a) Superimposition of flow curve obtained at 900 °C and 0.01 s^{-1} and the related variation of work hardening rate with true strain, (b–e) microstructures obtained respectively at the points marked by letters B to E in (a).

which $\sigma = \sigma_c$ and is known as the initiation point of DRX. In the third region, θ decreases with a higher slop towards $\theta = 0$ at σ_p. Similarly, the strain at which DRX reaches the highest rate can be deduced from θ–ε curve as indicated in Fig. 4(a). The negative value of work hardening rate in Fig. 4(a) is associated with the flow softening due to DRX. Therefore, the minimum value of θ corresponds to the maximum softening rate. The relationship between the critical and peak strain calculated here can be expressed as $\varepsilon_c = 0.73\,\varepsilon_p$ which is in agreement with previous reports [23,24,8].

Fig. 4(b–e) represents the evolution of microstructure with the strains marked by the corresponding capital letters on the flow curve of Fig. 4(a). It is observed in Fig. 4(b) that at the onset of hot deformation microstructure is nearly equiaxed. However, the serrated boundaries of highly elongated grains as well as locally bulged HABs indicated by arrows in Fig. 4(c) are typical of the initiation of DRX at the critical strain. Fig. 4(d) exhibits the microstructure at the peak where coarse work hardened grains and fine dynamically recrystallized grains are coexistence. This kind of microstructure is termed as a "necklace structure". At higher strains, the fraction of DRX increases gradually at the expense of the deformed matrix so that a fully dynamically recrystallized structure is observed at the steady state region, Fig. 4(e).

Fig. 5 indicates the variation of peak stress with deformation temperature at different strain rates. It is seen that deformation resistance decreases with increasing temperature. Besides, the linear regression of curves using the least square fitting according to the hyperbolic sine constitutive equation can be used to calculate the value of apparent activation energy for the hot deformation of the studied alloy. The relationship between flow stress and the Zener–Hollomon parameter, embracing the influence of temper-

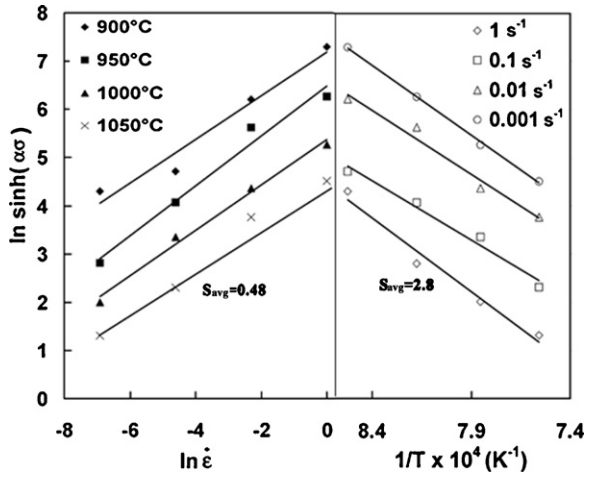

Fig. 5. Peak stress versus deformation temperature and strain rate in the frame of the hyperbolic sine equation.

ature, and strain rate is often described by the hyperbolic sine constitutive equation as follows [25–28]:

$$Z = \dot{\varepsilon} \exp\left(\frac{Q_{\text{def}}}{RT}\right) = A(\sinh(\alpha\,\sigma))^n \quad (1)$$

where Q_{def} denotes the apparent activation energy for deformation, R is the gas constant and n, α and A are material constants. Referring to Eq. (1), the stress exponent, n, is identified as the slope of strain rate vs. sin h($\alpha\sigma$) in a logarithmic scale. The stress multiplier α is an adjustable constant which makes the curves in Fig. 5 linear and parallel. The activation energy for hot deformation can be calculated using the derivative of the hyperbolic sine function of flow stress with respect to the reciprocal of temperature:

$$Q_{\text{def}} = Rn\left(\frac{\partial \ln \sinh(\alpha\,\sigma)}{\partial(1/T)}\right)_{\dot{\varepsilon}} \quad (2)$$

Using Eqs. (1) and (2), the values of α, n and the activation energy are determined as 0.02, 2.1 and 484 kJ/mol, respectively.

The peak and critical strains are plotted as a function of deformation temperature at different strain rates in Fig. 6(a–c). At strain rate of 0.001 s^{-1} (Fig. 6(a)), although the general trend of curves indicates the decrease peak and critical strain with increasing temperature, but an anomalous increase is observed at 1000 °C. The peak strain is constantly about 5% higher than the critical strain so that the mean ratio of $\varepsilon_c/\varepsilon_p$ is 0.67. At strain rate of 0.01 s^{-1} (Fig. 6(b)), the critical and peak strain decline with increasing temperature more quickly and the anomalous increase in the characteristic strains is observed at about 1100 °C. The ratio of $\varepsilon_c/\varepsilon_p$ is around 0.55. The same downward variation of the characteristic strains is observed for 0.1 s^{-1} where the anomalous increase in the characteristic strains occurs at 1150 °C, Fig. 6(c). In this case, the discrepancy between the peak and critical strains is about 0.11 and the ratio of $\varepsilon_c/\varepsilon_p$ is about 0.49. The decrease in $\varepsilon_c/\varepsilon_p$ with increasing strain rate reflects the fact that DRX is generally delayed as the rate of deformation increases. In order to incorporate the influence of temperature and strain rate the critical and peak strains can be plotted against the Z parameter, as shown in Fig. 7(a) and (b). The values of Z were calculated using the value of Q_{def} determined from Eq. (2). As expected, both peak and critical strains increase with Z. However, the anomalous increase in the characteristic strains behavior is observed at the Z value of about $10^{14.3}$. It should be noted that as the strain rate is increased, the temperature at which the maximum deviation appears rises. In addition, the altitude of the deviation decreases slightly as the strain rate rises.

The occurrence of the observed deviation in DRX behavior can be predicted using the development of a mechanism map, Fig. 8.

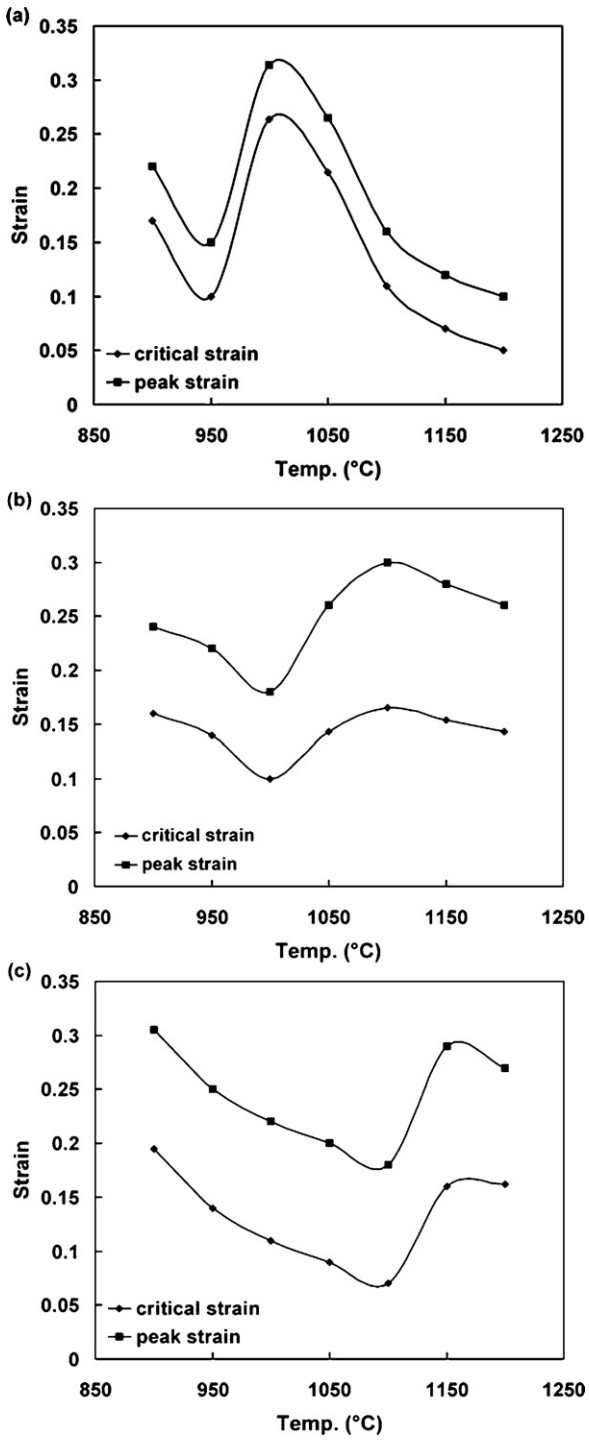

Fig. 6. Variation of peak and critical strains with deformation temperature at (a) 0.001 s^{-1}, (b) 0.01 s^{-1} and (c) 0.1 s^{-1}.

Four types of points as normal, lower boundary, upper boundary and abnormal were defined for each strain rate. The normal points were defined as points at which both the critical and peak strains lie on the expected trend curves. The lower boundary points were defined as the lowest temperatures at which at least one of the two values deviates from the expected curve. The upper boundary points represent the highest temperatures at which the same criterion is met and the abnormal points are those that lie between the two boundary lines. For all such points, the deviation for both strains was at least two times the error value.

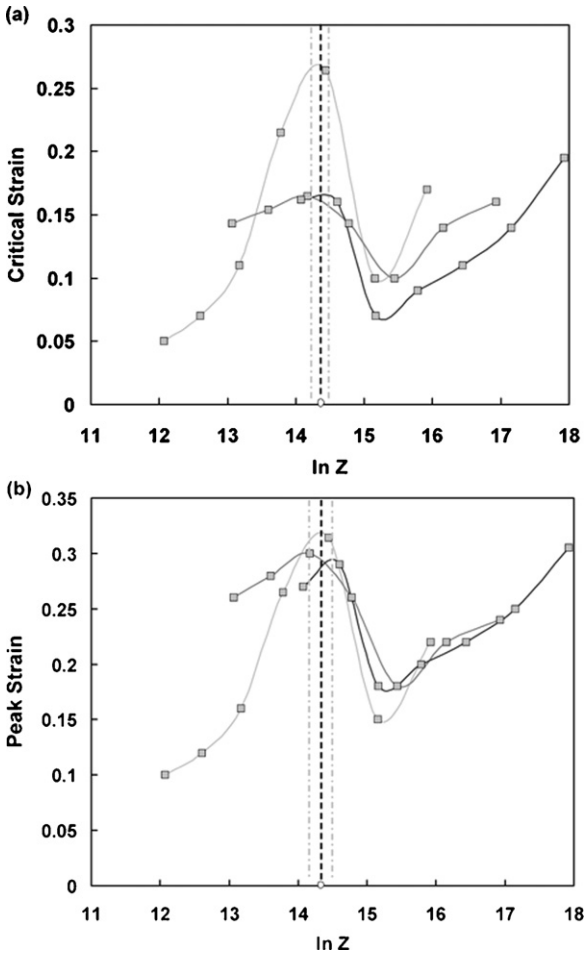

Fig. 7. Variation of (a) critical strain and (b) peak strain with the Zener–Hollomon parameter.

The best linear fit to the lower temperature boundary points is met if the activation energy takes the value of 385 ± 54 kJ/mol. Similarly, for the upper temperature boundary points the activation energy should be about 420 ± 40 kJ/mol. None of the calculated activation energies could be related to any particular physical phenomenon. However, as it will be discussed below this is not surprising because the overall effect probably involves a number of competing or overlapping temperature-dependent processes.

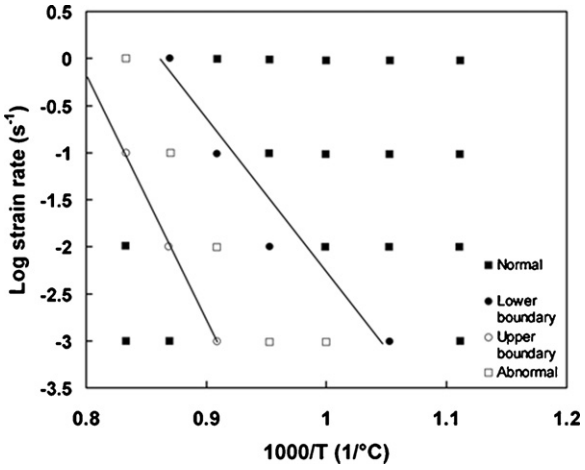

Fig. 8. Mechanism map derived to predict the regions of normal and abnormal DRX behavior in terms of the deformation variables.

It is worthy of note that both the critical and peak strains are affected in the region of abnormal behavior and the deformation conditions that lead to deviations are essentially identical. Furthermore, the relationship between the critical and peak strains, both in absolute ($\varepsilon_p - \varepsilon_c$) and relative ($\varepsilon_{p/}\varepsilon_c$) terms is met in the abnormal range. Therefore, it is concluded that the initiation of DRX is actually suppressed under the deviating deformation conditions. It is very well known that solute atoms and precipitation of second phase particles can delay or even hinder DRX [1,13]. In the absence of second phase particles, the probable mechanism responsible for the anomalous increase in the characteristic strains is therefore the segregation of solutes to the boundaries being involved in the nucleation of DRX grains. The segregation of solute atoms to the grain boundaries seems to exert a dragging force on the local bulges which tend to contribute in the initiation of DRX. As the segregating solute atoms can exert a dragging pressure without an actual pinning effect on the moving boundaries, DRX resumes when the critical amount of stored strain energy (i.e. the critical strain) necessary to overcome the dragging effect is provided.

The driving force for DRX or in other words grain boundary movement depends strongly on temperature and strain rate. Moreover, increasing temperature or decreasing strain rate lowers the driving force for DRX because they accelerate the annihilation of dislocations by dynamic recovery. The mobility of boundaries contributing in the nucleation of recrystallization is also a function of diffusion and therefore increases as deformation temperature rises. On the other hand, the diffusivity of segregating impurities increases and the driving force for segregation decreases as the deformation temperature rises. This is why the abnormal behavior is often observed over a specific temperature range which also depends on strain rate.

At lower temperatures (which correspond to the right-hand "normal" points in Fig. 8), the diffusion rate of impurity elements such as phosphorous are low and the accumulation rate of stored dislocation energy is high (as indicated by the higher flow stresses). Therefore, the rate of segregation is not enough to significantly interfere with the moving boundaries contributing in the initiation of dynamic recrystallization. At sufficiently high temperatures (the left-hand "normal" points in Fig. 8), boundary mobility is high enough to break away from the pinning solutes. The higher diffusivity of solute atoms helps this process. The increased mobility of the boundaries at the higher temperatures also coincides with diminished segregation driving forces, which in turn correspond to lower segregation level. At the intermediate temperatures (the abnormal and boundary points in Fig. 8), the rate of segregation is sufficiently high and the intrinsic mobility of the boundaries is low giving rise an appreciable interaction between them. When strain rate increases the driving force for DRX augments rapidly so that grain boundaries tend to move to annihilate the excess amount of dislocation. Therefore, at higher strain rates the interaction of solutes and moving boundaries occurs at higher temperatures where solute atoms can diffuse more rapidly and can keep pace with the moving boundaries.

The elements responsible for the observed anomalous phenomena are supposed to be silicon and phosphorus. The absence of the retardation effect in the high-purity stainless steels eliminates Cr, Ni and Mo as the potential causes of the deviations. Manganese can likewise be excluded, as its segregation behavior in austenite (specifically, its segregation driving force and diffusivity) is very similar to that of Cr and Ni. This leaves S, Si and P as the potential causes for the observed interaction with DRX.

Silicon has an intermediate misfit in austenite and the studied steel contains over 0.5% Si. However, the atomic radius of silicon is considerably larger than that of phosphorus or sulfur. This is why silicon atoms have a lower diffusivity in austenite comparing to phosphorus or sulfur. The investigation of equilibrium grain-

boundary segregation in a commercial 304 stainless steel at 1050 °C has showed that both sulfur and phosphorus appears significantly greater than silicon at grain boundaries [27].

Sulfur and phosphorus exhibit similar segregating behaviors in austenite, comparable diffusivities, similar segregation energies (sulfur is slightly higher) and nearly identical diffusion kinetics [29].

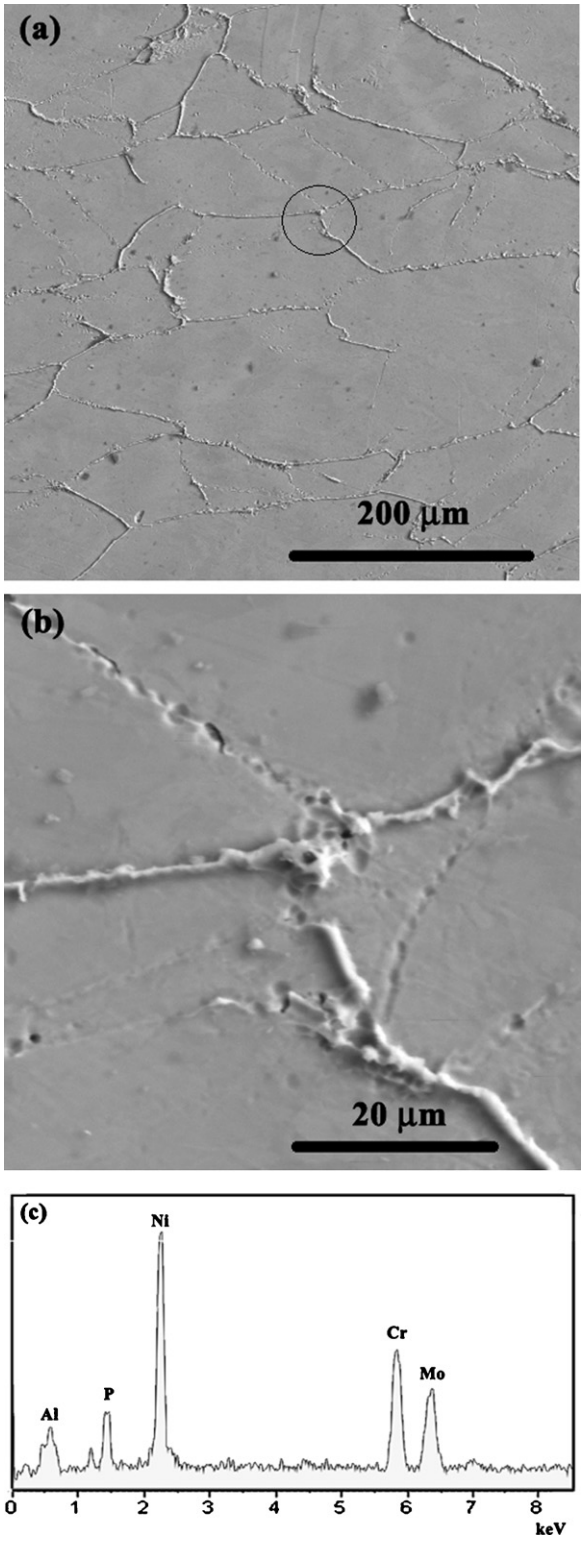

Fig. 9. (a) SEM micrograph of specimen hot deformed at 1100 °C and 0.001 s^{-1}, (b) magnified view of the area enclosed by a circle in (a) and (c) EDX microanalysis of the grain boundaries shown in (b).

Although the retardation of DRX may be due to the combined effects of these substitutionals, it is supposed that sulfur and silicon are minor contributors to the present effect as compared to phosphorus. Because, the studies of Fe–Si–P alloys have shown that the segregation enrichment ratio of phosphorus is almost 200 times greater than that of silicon in austenite [28]. In order to characterize the concentration of each segregating element the EDX microanalysis was performed on the specimens deformed in the anomalous region. Fig. 9 indicates the SEM micrograph and grain boundary microanalysis obtained from the specimen hot deformed at 1100 °C and 0.001 s^{-1}. It manifests that among the mentioned segregating elements, phosphorous has higher concentration and therefore accounts for the observed retardation of DRX.

4. Conclusions

The microstructural observations of grain boundary bulging as well as the analysis of work hardening rate at different flow stress were used to determine the critical strain for the initiation of dynamic recrystallization. The critical strain was found 0.5–0.7 times the peak strain of flow curve.

The empirical data of flow stress were successfully fitted to the hyperbolic sine function and the value of the apparent activation energy was determined about 484 kJ/mol.

The critical and peak strains for dynamic recrystallization deviated from the expected decreasing trend with increasing temperature. The anomalous rise in critical/peak strain appeared at higher temperatures as the strain rate increased. This approach introduced a DRX retardation process which was dominated when $\ln Z$ was in range of 13–15. The retardation behavior was maximized at about $\ln Z = 14.3$.

The EDX microanalysis of grain boundaries at the deviating hot deformation temperatures confirmed that the segregation of substitutional impurities, *P* in particular, to grain boundaries was responsible for the observed retardation of DRX.

References

[1] A. Momeni, K. Dehghani, H. Keshmiri, G.R. Ebrahimi, Mater. Sci. Eng., A 527 (2010) 1605–1611.
[2] S. Venugopal, S.L. Mannan, P. Rodriguez, J. Mater. Sci. 39 (2004) 5557–5560.
[3] A. Dehghan-Manshadi, P.D. Hodgson, J. Mater. Sci. 43 (2008) 6272–6277.
[4] M. El Wahabi, L. Gavard, F. Montheillet, J.M. Cabrera, J.M. Prado, Acta Mater. 53 (2005) 4605–4612.
[5] A. Momeni, A. Shokuhfar, S.M. Abbasi, J. Mater. Sci. Technol. 23 (2007) 775–778.
[6] A. Dehghan-Manshadi, M.R. Barnett, P.D. Hodgson, Mater. Sci. Eng. A485 (2008) 664–672.
[7] R. Ding, Z.X. Guo, Acta. Mater. 49 (2001) 3163–3175.
[8] S.H. Cho, Y.C. Yoo, J. Mater. Sci. 36 (2001) 4267–4272.
[9] H.J. McQueen, E. Evangelista, N.D. Ryan, in: T. Chandra (Ed.), Recrystallization in Metals and Materials, AIME, Warrendale, PA, 1990, pp. 89–100.
[10] R. Ding, Z.X. Guo, Acta Mater. 49 (2001) 3163–3175.
[11] X. Wang, E. Brunger, G. Gottstein, Mater. Sci. Eng. A290 (2000) 10–185.
[12] S. Mandal, P.V. Sivaprasad, R.K. Dube, J. Mater. Sci. 42 (2007) 2724–2734.
[13] S.I. Kim, D.J. Baek, Y. Lee, S.H. Choi, Mater. Sci. Forum 500–501 (2005) 321–328.
[14] S.I. Kim, S.H. Choi, Y. Lee, Mater. Sci. Eng. A406 (2005) 125–133.
[15] L. Gavard, F. Montheillet, J. Le Coze, Mater. Trans. JIM 41 (2000) 113–115.
[16] A. Momeni, S.M. Abbasi, A. Shokuhfar, J. Iron Steel Res. Int. 14 (2007) 66–70.
[17] A. Momeni, S.M. Abbasi, Mater. Des. 31 (2010) 3599–3604.
[18] A. Momeni, K. Dehghani, G.R. Ebrahimi, H. Keshmiri, Met. Mater. Trans. 41A (2010) 2898–2904.
[19] J.J. Jonas, E.I. Poliak, Mater. Sci. Forum 426–432 (2003) 57–66.
[20] E.I. Poliak, J.J. Jonas, ISIJ Int. 43 (2003) 684–691.
[21] S.I. Kim, Y.C. Yoo, Mater. Sci. Technol. 18 (2002) 160–164.
[22] A. Manonukul, F.P.E. Dunne, Acta Mater. 47 (1999) 4339–4354.
[23] Y.C. Yoo, J.S. Jeon, B.C. Ko, Mater. Sci. Forum 217–222 (1996) 1157–1162.
[24] S.I. Kim, S.H. Cho, Y.C. Yoo, The Third European Congress of Stainless Stee1'99 Science and Market, Chia Laguna Sardinia, Italy, 1999, pp. 423–428.
[25] A. Momeni, K. Dehghani, Mater. Sci. Eng. A527 (2010) 5467–5473.
[26] A. Momeni, K. Dehghani, Met. Mater. Int. 16 (2010) 843–849.
[27] A. Joshi, D.F. Stein, Corrosion 28 (1972) 321–330.
[28] P. Lejcek, S. Hofmann, Surf. Interface Anal. 16 (1990) 546–553.
[29] R.G. Faulkner, Mater. Sci. Technol. 1 (1985) 442–447.